


Article

Effects of Cobalt Content on the Microstructure, Mechanical Properties and Cavitation Erosion Resistance of HVOF Sprayed Coatings

Ji Liu ¹, Xiuqin Bai ^{1,*}, Tongzhou Chen ² and Chengqing Yuan ¹ 

¹ Reliability Engineering Institute, National Engineering Research Center for Water Transport Safety, Wuhan University of Technology, Wuhan 430063, China

² State Key Laboratory of Special Surface Protection Materials and Application Technology, Wuhan Research Institute of Materials Protection, Wuhan 430030, China

* Correspondence: xqbai@whut.edu.cn

Received: 29 July 2019; Accepted: 20 August 2019; Published: 22 August 2019



Abstract: Cobalt-based alloy coatings and WC-Co-based ceramic–metal (cermet) coatings have been widely used because of their desirable mechanical properties and corrosion resistance. In this work, the influence of Co content on the microstructure, mechanical properties and cavitation erosion (CE) resistance were investigated. A cobalt-based alloy coating, a WC-12Co coating, and a WC-17Co cermet coating were deposited by high-velocity oxygen fuel (HVOF) spraying on 1Cr18Ni9Ti substrates. Results indicate that the cobalt-based alloy coating had the largest surface roughness because surface-bonded particles of lower plastic deformation were flattened. The existence of WC particles had led to an increase in hardness and improved the fracture toughness due to inhibit crack propagation. The pore appeared at the interface between WC particles, and the matrix phase had introduced an increase in porosity. With the increase in Co content, the cohesion between matrix friction and WC particles increased and then decreased the porosity (from 0.99% to 0.84%) and surface roughness (R_a from 4.49 to 2.47 μm). It can be concluded that the hardness had decreased (from 1181 to 1120 $\text{HV}_{0.3}$) with a decrease in WC hard phase content. On the contrary, the fracture toughness increased (from 4.57 to 4.64 $\text{MPa}\cdot\text{m}^{1/2}$) due to higher energy absorption in the matrix phase. The WC-12Co and WC-17Co coatings with higher hardness and fracture toughness exhibited better CE resistance than the cobalt-based alloy coating, increasing more than 20% and 16%, respectively. Especially, the WC-12Co coating possessed the best CE resistance and is expected to be applicable in the hydraulic machineries.

Keywords: cobalt-based alloy; WC-Co; cobalt content; HVOF; mechanical properties; cavitation erosion

1. Introduction

A cobalt-based alloy coating is widely used to protect materials against wear, cavitation erosion (CE), and corrosion because of their higher hardness, strength, and better corrosion resistance. The cobalt-based alloys (such as Stellite 6 or Stellite 12) consist of fcc cobalt-based dendrites with interdendritic lamella of Cr-rich carbides, which provide the alloy with the hardness to resist CE [1]. Multiphase materials composed of a metallic matrix reinforced by the distribution of hard particles are also extensively used to enhance toughness and hardness [2,3] and to improve the resistance of CE [4], wear [5], and slurry erosion [6].

To improve the CE resistance of material, high-velocity air fuel [7], high-velocity oxygen fuel (HVOF) [8], arc spraying [9], atmospheric plasma spraying [10], and other surface modification technologies had been developed. Due to the optimal combination of mechanical strength (hardness

and fracture toughness), HVOF-sprayed WC-Co-based ceramic–metal (cermet) composites coatings can improve CE resistance [11,12]. Lamana et al. [13] demonstrated that an increase in Co content could lead to an increase in the fracture toughness and CE resistance of WC-Co coatings, which also resulted from the increase in compressive residual stress. Chivavibul et al. [14] prepared WC-Co coatings with different cobalt contents (8 wt.%, 12 wt.%, 17 wt.% and 25 wt.%) by HVOF spraying, and they found that the hardness and Young’s modulus decreased with an increase in cobalt content, but the fracture toughness did not show noticeable changes. Thus, the mechanical properties and CE resistance affected by the cobalt content are still needed to be further studied.

In this study, the effects of the presence of WC particles on the formation, surface morphologies, mechanical properties and CE resistance of the coatings were evaluated. A cobalt-based alloy coating and two kinds of WC-Co cermet coatings were prepared with HVOF spraying on 1Cr18Ni9Ti substrates. Furthermore, two WC-Co cermet coatings with different Co contents were selected to analyze the effect of matrix phase content on microstructure features, mechanical properties and CE resistance.

2. Methodology

2.1. Materials and HVOF Spraying Procedure

The composition of the sprayed commercial cobalt-based alloy powder is listed in Table 1. The chemical composition (wt.%) of the cermet feedstock powders used were 88WC-12Co and 83WC-17Co. The cobalt-based alloy powder was prepared from gas atomization, and the WC-12Co and WC-17Co powders were prepared by agglomeration and sintering. The fraction sizes of the three kinds of powders used were 15–45 μm .

Table 1. Composition of the cobalt-based alloy powder.

Element	C	Si	Cr	Mn	Mo	Fe	Ni	W	Co
wt.%	0.25	1.50	27.30	≤ 0.50	≤ 5.50	1.50	2.00	≤ 0.50	Balance

The cobalt-based alloy coating, the WC-12Co coating, and the WC-17Co coating were deposited by a HVOF spraying system with a K2 gun (GTV, Luckenbach, Germany). The spray distance was approximately 420 mm, and the powder feed rate was 100 g/min. The oxygen and kerosene flow rate were 950 and 22 L/min, respectively. The 1Cr18Ni9Ti substrate samples were degreased and grit blasted ($R_a \approx 4 \mu\text{m}$), and they were then cleaned by using acetone in an ultrasonic bath.

2.2. Coating Characterization and Property Tests

The morphologies of the three kinds of powders and as-sprayed coatings were investigated using a VEGA3 (TESCAN, Brno, Czech Republic) scanning electron microscope (SEM). Five cross-sectional images were taken for each sample to evaluate the thickness, and twenty images were taken for the porosity via the Image J software package (version 1.8.0). The surface roughness (R_a , R_z) of the coatings was measured with a VK-X1000 (KEYENCE, Osaka, Japan) laser scanning confocal microscopy. The phase composition of coatings was determined using a D8 Advance (BRUKER, Ettlingen, Germany) X-ray diffraction (XRD), using Cu-K α at a voltage of 45 kV, current of 40 mA, and 2θ was between 30° and 90° .

2.3. Mechanical Testing

The hardness of coatings was determined by an MVD-1000JMT2 Vickers hardness tester (JMTT, Shanghai, China) on the polished cross section. The test was conducted under a 2.94 N load with a dwell time of 10 s, and the average hardness value was obtained from ten indentations.

Fractures were made on the cross section with an AVK-A Vickers hardness tester (AKASHI, Kyoto, Japan). The measurements were carried out using a Vickers indenter for 10 s at a load of 49 N.

The indentation crack parallel to the interface on the cross section of the coating is shown in Figure 1. The results were the average value of five measurements for each sample. The fracture toughness (K_C) value was calculated according to the Evans–Wilshaw equation [15].

$$K_C = 0.079 \left(\frac{P}{a^{3/2}} \right) \log \left(\frac{4.5a}{c} \right) \quad (1)$$

where P is the indentation load (mN), $2c$ is the crack length (μm), and $2a$ is the diagonal length of the indentation (μm).

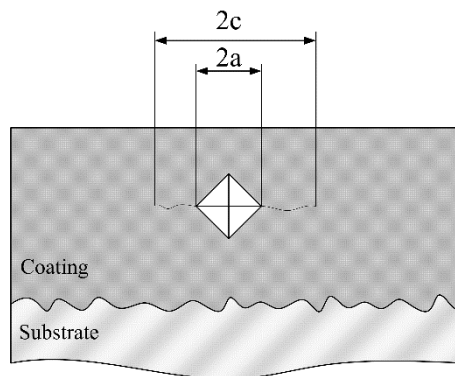


Figure 1. Schematic of fracture toughness measurement with Vickers indentation.

2.4. Cavitation Erosion Tests

The CE tests were conducted on the substrate and three kinds of coatings in deionized water according to ASTM G32-16 [16]. Cavitation erosion equipment was conducted at 20 kHz and a peak-to-peak amplitude of 25 μm . The deionized water temperature was kept at 25–30 $^{\circ}\text{C}$. The specimen (diameter 25 mm, thickness 8 mm) surface was immersed in deionized water with a 3 mm depth. The sample was tested for 480 min, the mass loss was weighed with a balance (0.1 mg accuracy) every 30 min, and the volume loss was calculated by divided the measured mass loss by the density. The volume loss was calculated using three same samples in order to confirm reproducibility. The density of 1Cr18Ni9Ti substrate was 7.85 $\text{g}\cdot\text{cm}^{-3}$.

3. Results

3.1. Microstructure

SEM images of the cobalt-based alloy powder, WC-12Co powder, and WC-17Co powder are depicted in Figure 2. The WC-12Co and WC-17Co powders were a near-spherical shape with a few pores. The cobalt-based alloy powders had regular spherical shapes and almost no pores.

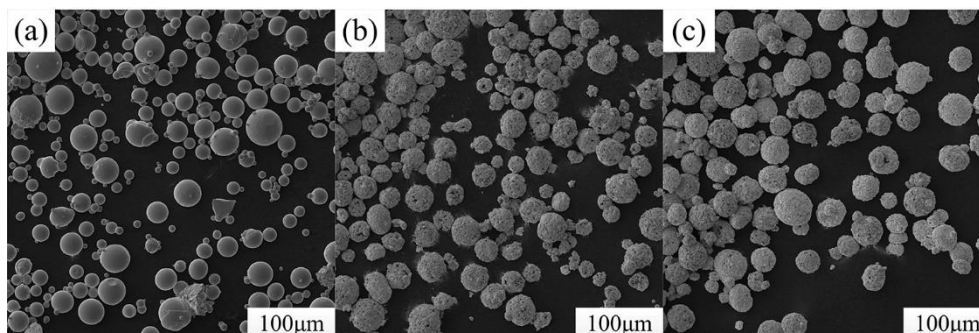


Figure 2. SEM images of feedstock powders: (a) Cobalt-based alloy, (b) WC-12Co, and (c) WC-17Co.

The cross-sectional images of the coatings are shown in Figure 3. The interface between the substrate and both WC-12Co and WC-17Co coatings was obvious, but it was not so clear in the cobalt-based alloy coating (Figure 3(a-1)). It could be seen that several pores existed in the WC-12Co and WC-17Co coatings (Figure 3(b-2,c-2)), while the cobalt-based alloy coating had dense microstructures (Figure 3(a-2)). The polygon WC particles distributed in the matrix phase of the WC-12Co coating had much larger size variation, while the microstructure of the WC-17Co coating contained much finer WC particles. The dark gray binder matrix phase in the WC-17Co coating was more than that in the WC-12Co coating, and a higher fraction of WC particles were observed in the WC-12Co coating.

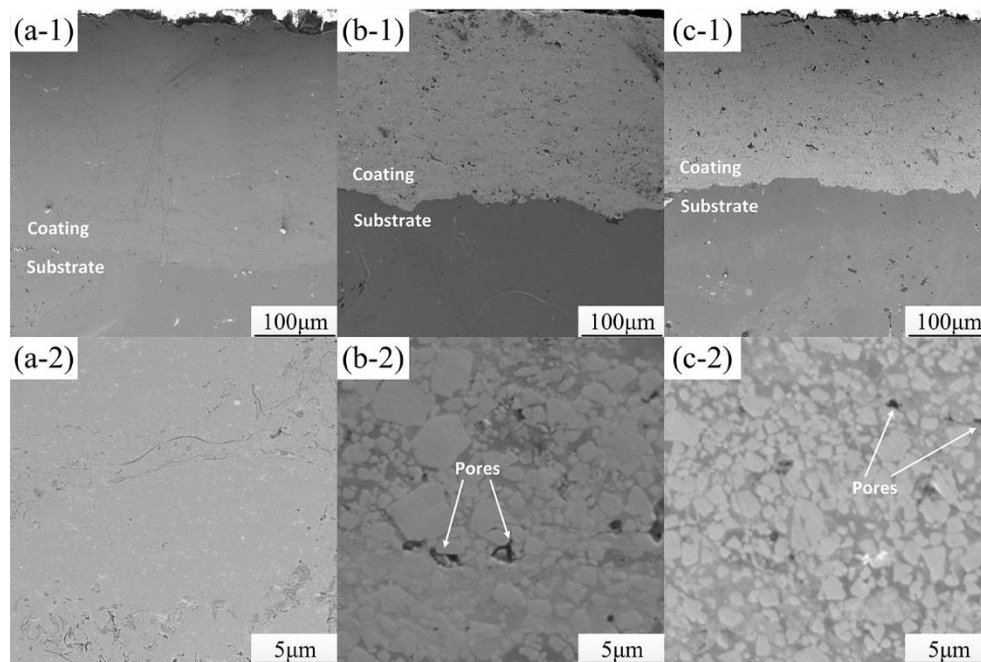


Figure 3. Cross-sectional microstructures of the coatings: Cobalt-based alloy at low-magnification (a-1) and high-magnification (a-2); WC-12Co at low-magnification (b-1) and high-magnification (b-2); WC-17Co at low-magnification (c-1) and high-magnification (c-2).

The measured average thicknesses of the cobalt-based alloy coating, the WC-12Co coating, and the WC-17Co coating were 300 ± 9 , 232 ± 9 and 221 ± 6 μm , respectively. The cobalt-based alloy coating had the maximum thickness. This is because the density of the powder was lower than the other two coatings.

Figure 4 shows the 3D surface morphologies and the surface properties of the three coatings. Figure 4c shows that the surface morphology of the WC-17Co coating was relatively flatter than the other two coatings and the WC-12Co coating surface contained several finer particles (Figure 4b). However, it was observed that several bulges (dark red area) appeared on the surface of the cobalt-based alloy coating (Figure 4a). Because the shapes and dimensions of the bulges were close to that of the feedstock powders, it could be deduced that the bulges were the slight flat particles.

According to Figure 4d, the WC-17Co coating showed the lowest surface roughness, followed by the WC-12Co and cobalt-based alloy coatings. The porosities of the WC-12Co and WC-17Co coatings were less than 1%, while the cobalt-based alloy coating was below 0.4% (Figure 4d). The values of surface roughness were consistent with the surface morphologies. The WC-12Co and WC-17Co coatings had higher porosity because pores were present in the interfaces between the WC particles and the matrix phase (Figure 3(b-2, c-2)).

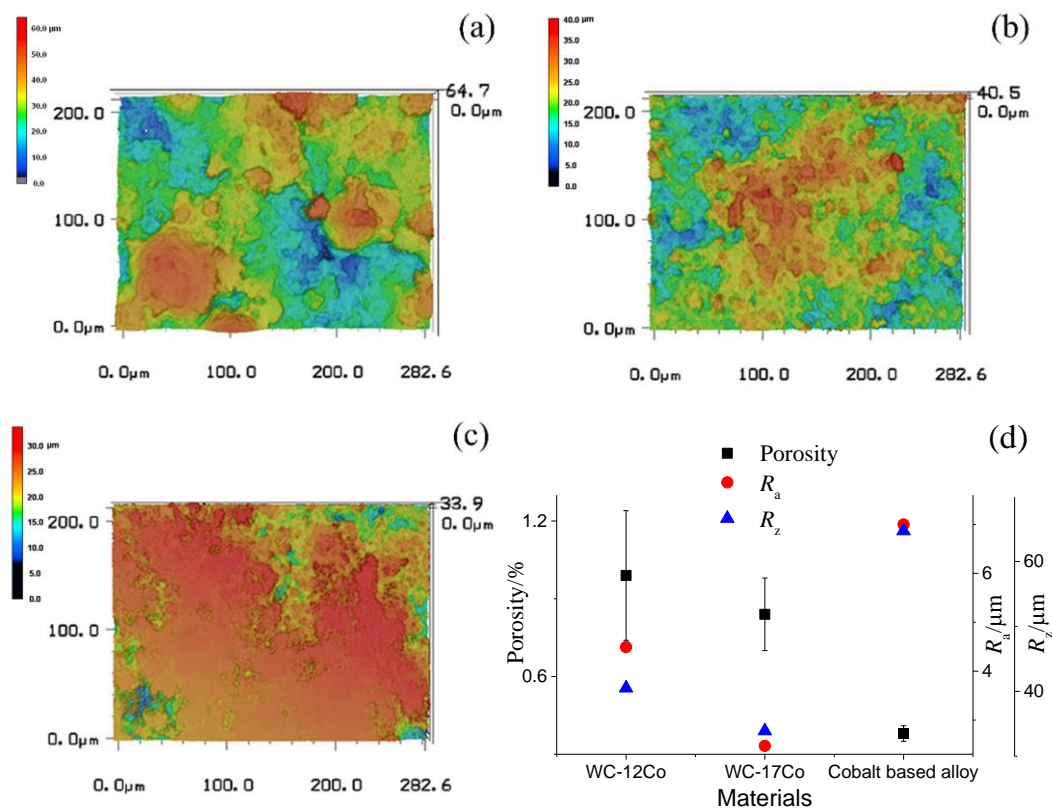


Figure 4. 3D surface morphologies of the coatings: (a) Cobalt-based alloy, (b) WC-12Co, and (c) WC-17Co. (d) The porosity and surface roughness of the coatings.

3.2. Mechanical Properties

The average microhardness and fracture toughness values of the three coatings are illustrated in Figure 5. The microhardness of the cobalt-based alloy coating was 553 HV_{0.3}, while the fracture toughness was 2.58 MPa·m^{1/2}. For the WC-12Co and WC-17Co coatings, the hardness values increased more than 77% and 79%, respectively, than the cobalt-based alloy coating. Meanwhile, the fracture toughness was higher than 77% and 79%. With increases of Co content in the two cermet coatings, the fracture toughness value showed a slight increase, but the hardness value decreased slightly, ranging from 1181 to 1120 HV_{0.3}.

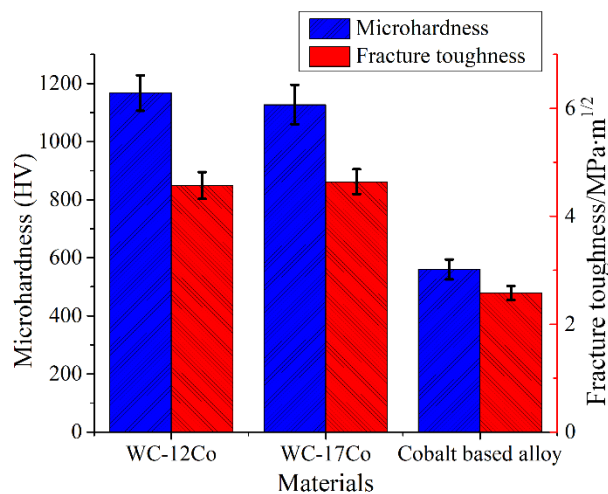


Figure 5. The microhardness and fracture toughness of the coatings.

Figure 6 shows that the indentation cracks initiated from the edge of the Vickers indenter tip and parallel to the interface. Two major cracks propagated parallel to the interface were observed, and the negligible level of secondary cracks were found in the vicinity of indentations.

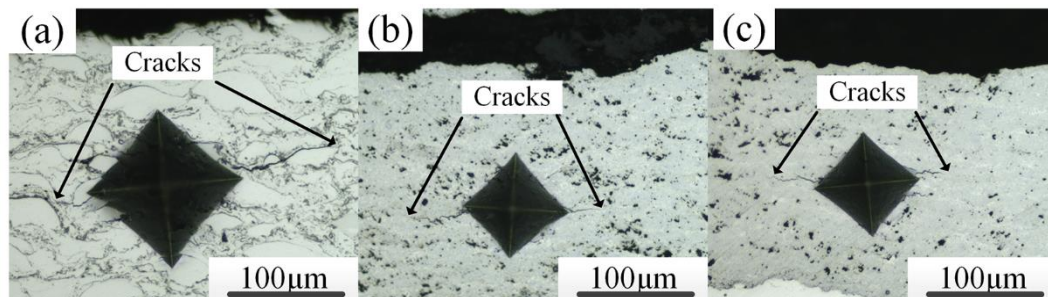


Figure 6. Micrographs of fracture toughness of the coatings: (a) Cobalt-based alloy, (b) WC-12Co, and (c) WC-17Co.

3.3. Cavitation Erosion Behavior

The CE results of substrate, cobalt-based alloy coating, the WC-12Co coating, and the WC-17Co coating in deionized water are presented in Figure 7. As shown in Figure 7a, all the coatings had a high volume loss rate in the initial stage (30 min), and then the two cermet coatings reached the relatively steady-state, but the cobalt-based alloy coating still exhibited a larger fluctuation. The cumulative volume loss curves of the coatings are illustrated in Figure 7b. It can be seen that the cermet coatings had superior CE resistance than the cobalt-based alloy coating. The CE resistance of the WC-12Co and WC-17Co coatings increasing more than 20% and 16%, respectively, compared with the cobalt-based alloy coating. As shown in Figure 7b, the cermet coatings presented better CE resistance than the substrate.

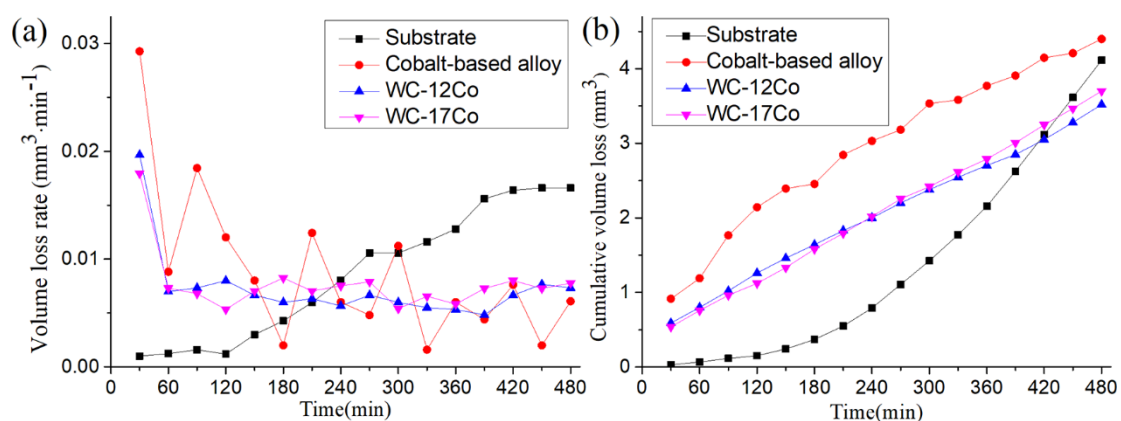


Figure 7. Volume loss of the coatings in deionized water: (a) volume loss rate and (b) cumulative volume loss.

4. Discussion

The measured surface roughness of the cobalt-based alloy coating was higher than the WC-12Co and WC-17Co cermet coatings. It can be observed from Figure 4a that slight-flat particles had formed on the surface of the cobalt-based alloy coating. However, slight-flat particles did not appear in the inner parts of the coating, as shown in Figure 3(a-2). It can be explained that the inner particles impinging on the ductile substrate were easily deformed and flattened. On the contrary, the surface-bonded particles possessed lower plastic deformation because the coating material had larger stiffness [17]. Therefore, the inner particles had higher densification, but the surface impinged particles had slight flattening.

For the WC-12Co and WC-17Co cermet coatings, the surface roughness and porosity decreased with increasing Co content. The cohesion between the matrix friction and WC particles increased, thereby decreasing the porosity and the surface roughness. On the other hand, the size of the WC particles in the WC-17Co coating was uniform and smaller than the WC-12Co coating. Some studies [11,18] have indicated that a smaller WC particle size is desirable in decreasing porosity.

The obtained hardness value of cobalt-based alloy coating was 553 HV_{0.3}, which was attributed to the coating with the dense structure and the Co-based fcc-phase, as shown in Figure 8. The Cr-rich M₇C₃ phase was visible in the coating XRD patterns [19,20]. The hardness of the WC-12Co and WC-17Co coatings were found to be higher than that of the cobalt-based alloy coating, which was due to the distribution of the WC particles in the matrix friction that acted as a hardness reinforcement [21–24]. Meanwhile, the retention of solid WC particles could potentially increase the kinetic energy and improve coating compaction, thus leading to tighter inter-particle bonding and strong cohesion.

The hardness of the WC-12Co and WC-17Co cermet coatings decreased with increasing cobalt content because of the decrease in the WC hard phase content [25]. The hardness of the WC-12Co coating observed was slightly lower than those reported by other researchers [23,26]. It was noticed that the hardness of the coating was dependent on the microstructure, phase structure (amounts of W₂C, amorphous phase), porosity, peening effect, etc. [14]. The XRD results indicate that the difference between the two cermet coatings was negligible, as shown in Figure 8. It could be deduced the hardness of the WC-12Co coating was slightly lower than that reported, mainly because of the relatively higher porosity (0.99%).

Compared to the cobalt-based alloy coating, the existence of WC particles in the cermet coatings played an active role to improve the fracture toughness. In the crack extension process, the trans-granular fracture, deflecting, and branching effect could inhibit crack propagation and improve the fracture toughness of the cermet coatings. The fracture toughness slightly increased with increasing Co content for the two cermet coatings because the ductile matrix phase had higher energy absorption than the WC particles and then hindered the crack to grow and propagate [13,14,25]. The fracture toughness of the cross section was related to the properties of the lamella interfaces [15]. The higher fracture toughness meant better lamellar cohesion, which was attributed to the HVOF with high-velocity particles that also caused the sprayed coating with less porosity [13,15]. On the contrary, the high level of porosity facilitated crack propagation and decreased the fracture toughness of the coating [2]. Therefore, it can be concluded that high fracture toughness resulted from the higher fraction of matrix phase, and the minor porosity provided a greater lamellar cohesion.

The CE rate of the three kinds of coatings in the initial stage (30 min) were consistent with the values of surface toughness (Figure 7a). At 60 min, the coatings presented a lower CE rate, and the cermet coatings showed a smaller fluctuation in latter tests. It can be revealed that the surface roughness affected the CE rate only in the initial stage (30 min).

Figure 9 exhibits the surface morphologies of coatings after 480 min of CE tests in deionized water. The cobalt-based alloy coating presented the surface crater, which was caused by the un-molten particle fallen off (Figure 9(a–2)). The surface of the WC-17Co coating had more serious CE damage than the WC-12Co coating, and both of them appeared with craters and exposed WC particles (Figure 9(b–2, c–2)).

The cermet coatings exhibited better CE resistance than the cobalt-based alloy coating (Figure 7b), which was attributed to their higher hardness and fracture toughness. The higher hardness of the coating could improve the CE resistance, and the fracture toughness reflected the ability to hinder and delay the generation and propagation of fatigue cracks during the CE process [13]. Meanwhile, the WC-12Co and WC-17Co coatings with higher hardness (1181 and 1120 HV_{0.3}) could counteract the negative influence of higher porosity (0.99% and 0.84%) on the CE resistance [27]. The WC-12Co coating exhibited a slightly superior CE resistance than the WC-17Co coating, because the WC-12Co coating possessed the higher hardness even though the WC-17Co coating had slight higher fracture toughness and lower porosity.

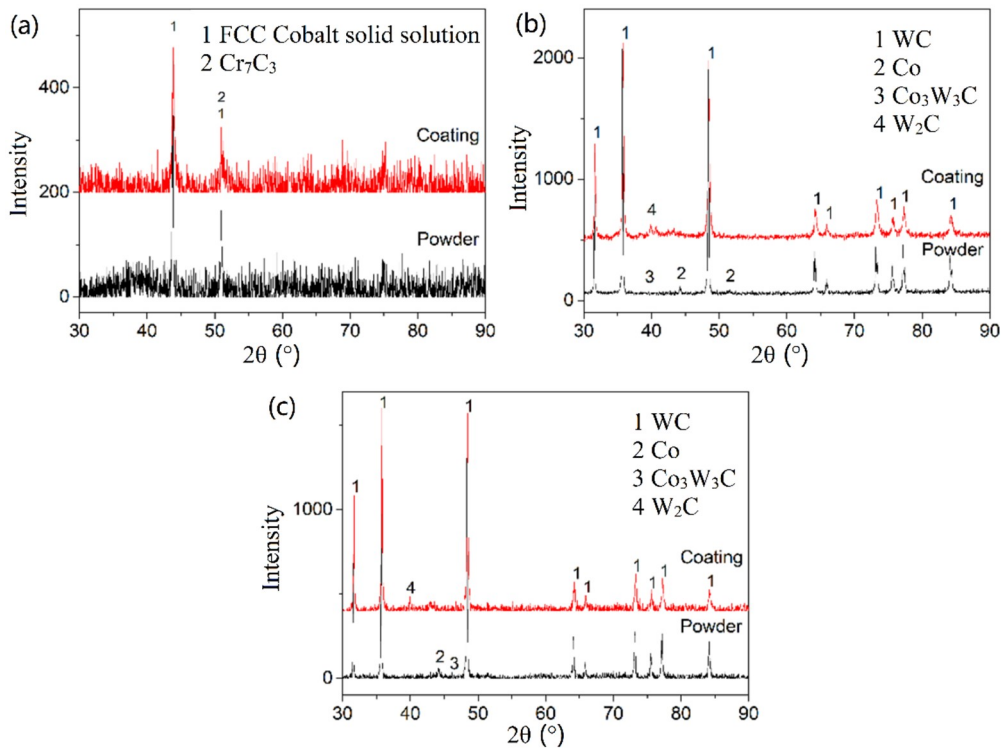


Figure 8. XRD patterns of the coatings: (a) Cobalt-based alloy, (b) WC-12Co, and (c) WC-17Co.

Therefore, the different cobalt contents affected the microstructure features and mechanical properties of the coatings, and they further influenced the CE resistance. The WC-12Co coating possessed high hardness and fracture toughness and is expected to be applicable to improve the CE resistance of hydraulic machineries.

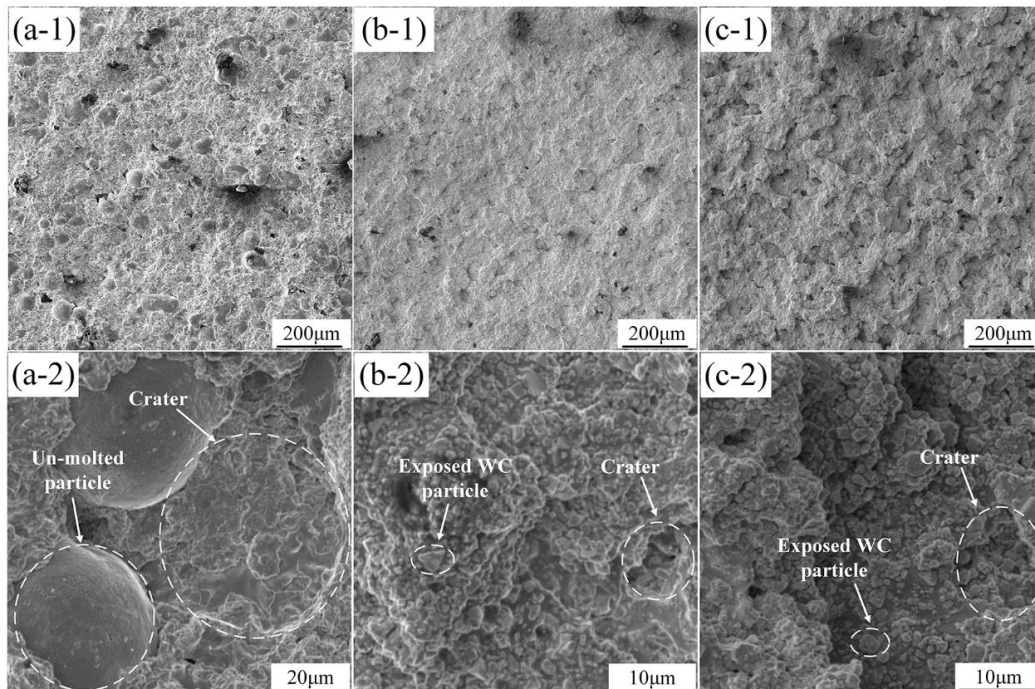


Figure 9. SEM images of eroded surfaces after cavitation test in deionized water: Cobalt-based alloy at low-magnification (a-1) and high-magnification (a-2); WC-12Co at low-magnification (b-1) and high-magnification (b-2); WC-17Co at low-magnification (c-1) and high-magnification (c-2).

5. Conclusions

A cobalt-based alloy and WC-Co-based cermet coatings were deposited by a HVOF spraying process. Their microstructure, mechanical properties, and CE resistance were evaluated. The following conclusions are drawn.

- The cobalt-based alloy coating has the largest surface roughness because surface-bonded particles with a lower plastic deformation contain slight flattening. For the cermet coatings, the existence of finer WC particles decreased the surface roughness, and it caused pores to appear at the interface between WC particles and the matrix phase. Their cohesion increased with the increase in Co content while the porosity (from 0.99% to 0.84%) and the surface roughness (R_a from 4.49 to 2.47 μm) decreased in the cermet coatings.
- The hardness value of the cobalt-based alloy coating was 553 $\text{HV}_{0.3}$, and this was attributed to the coating with the dense structure and the Co-based fcc-phase. The hardness of the WC-12Co (1181 $\text{HV}_{0.3}$) and WC-17Co (1120 $\text{HV}_{0.3}$) coatings were higher than the cobalt-based alloy coating because of the distribution of the WC particles in the matrix friction. The hardness slightly decreased with increasing Co content due to the decrease in WC hard phase content.
- The existence of WC particle resisted crack propagation and improved the fracture toughness in the cermet coatings. The fracture toughness slightly increased (from 4.57 to 4.64 $\text{MPa}\cdot\text{m}^{1/2}$) with increasing Co content for the cermet coatings. This is because the ductile matrix phase had higher energy absorption than the WC particles and hindered crack growth and propagation. The WC-17Co coating with minor porosity also provided a greater lamellar cohesion to improve the fracture toughness.
- The CE rate of the coatings in the initial stage was affected by the surface roughness. The WC-12Co and WC-17Co coatings with higher hardness and fracture toughness exhibited better CE resistance than the cobalt-based alloy coating, increasing more than 20% and 16%, respectively. The WC-12Co coating possessed a higher CE resistance than the WC-17Co coating because the hardness had a great influence on CE resistance. Especially, the WC-12Co coating possessed the best CE resistance and is expected to be applicable in the hydraulic machineries. Therefore, the effect of the ingredient added to cobalt-based coatings on the CE resistance are worth further study.

Author Contributions: Conceptualization, Methodology, Validation, Writing-Original Draft, J.L.; Methodology, Investigation, Resources, T.C.; Supervision, Project Administration, C.Y.; Conceptualization, Writing-Review and Editing, Visualization, Supervision, X.B.

Funding: This research received no external funding.

Conflicts of Interest: The authors declare no conflict of interest.

References

1. Sreedhar, B.K.; Albert, S.K.; Pandit, A.B. Improving cavitation erosion resistance of austenitic stainless steel in liquid sodium by hardfacing—Comparison of Ni and Co based deposits. *Wear* **2015**, *342*, 92–99. [[CrossRef](#)]
2. Nahvi, S.; Jafari, M. Microstructural and mechanical properties of advanced HVOF-sprayed WC-based cermet coatings. *Surf. Coat. Technol.* **2016**, *286*, 95–102. [[CrossRef](#)]
3. Zhang, Y.; Yu, F.; Hao, S.; Dong, F.; Xu, Y.; Geng, W.; Zhang, N.; Gey, N.; Grosdidier, T.; Dong, C. Evolution of nanostructure and metastable phases at the surface of a HCPEB-treated WC-6% Co hard alloy with increasing irradiation pulse numbers. *Coatings* **2017**, *7*, 178. [[CrossRef](#)]
4. Wang, Q.; Tang, Z.; Cha, L. Cavitation and sand slurry erosion resistances of WC-10Co-4Cr coatings. *J. Mater. Eng. Perform.* **2015**, *24*, 2435–2443. [[CrossRef](#)]
5. Suo, X.; Yin, S.; Li, H.; Lupoi, R. Numerical and experimental investigation on bonding behavior of cold sprayed porous WC-17Co particles onto different substrates. *Coatings* **2018**, *8*, 367. [[CrossRef](#)]
6. Kumar, K.; Kumar, S.; Singh, G.; Singh, J.P.; Singh, J. Erosion wear investigation of HVOF sprayed WC-10Co4Cr coating on slurry pipeline materials. *Coatings* **2017**, *7*, 54. [[CrossRef](#)]

7. Wang, Q.; Zhang, S.; Cheng, Y.; Xiang, J.; Zhao, X.; Yang, G. Wear and corrosion performance of WC-10Co4Cr coatings deposited by different HVOF and HVAF spraying processes. *Surf. Coat. Technol.* **2013**, *218*, 127–136. [[CrossRef](#)]
8. Milanti, A.; Koivuluoto, H.; Vuoristo, P.; Bolelli, G.; Bozza, F.; Lusvarghi, L. Microstructural characteristics and tribological behavior of HVOF-sprayed novel Fe-based alloy coatings. *Coatings* **2014**, *4*, 98–120. [[CrossRef](#)]
9. Lin, J.; Wang, Z.; Cheng, J.; Kang, M.; Fu, X.; Hong, S. Effect of Initial Surface Roughness on cavitation erosion resistance of arc-sprayed Fe-based amorphous/nanocrystalline coatings. *Coatings* **2017**, *7*, 200. [[CrossRef](#)]
10. Shi, Z.; Wang, J.; Wan, Z.; Qiao, Y.; Xiong, T.; Zheng, Y. Cavitation erosion and jet impingement erosion behavior of the NiTi coating produced by air plasma spraying. *Coatings* **2018**, *8*, 10. [[CrossRef](#)]
11. Ding, X.; Ke, D.; Yuan, C.; Ding, Z.; Cheng, X. microstructure and cavitation erosion resistance of HVOF deposited WC-Co coatings with different sized WC. *Coatings* **2018**, *8*, 307. [[CrossRef](#)]
12. Ding, X.; Cheng, X.D.; Shi, J.; Li, C.; Yuan, C.Q.; Ding, Z.X. Influence of WC size and HVOF process on erosion wear performance of WC-10Co4Cr coatings. *Int. J. Adv. Manuf. Technol.* **2018**, *96*, 1615–1624. [[CrossRef](#)]
13. Lamana, M.S.; Pukasiewicz, A.G.; Sampath, S. Influence of cobalt content and HVOF deposition process on the cavitation erosion resistance of WC-Co coatings. *Wear* **2018**, *398*, 209–219. [[CrossRef](#)]
14. Chivavibul, P.; Watanabe, M.; Kuroda, S.; Shinoda, K. Effects of carbide size and Co content on the microstructure and mechanical properties of HVOF-sprayed WC-Co coatings. *Surf. Coat. Technol.* **2007**, *202*, 509–521. [[CrossRef](#)]
15. Varis, T.; Suhonen, T.; Ghabchi, A.; Valarezo, A.; Sampath, S.; Liu, X.; Hannula, S.P. Formation mechanisms, structure, and properties of HVOF-sprayed WC-CoCr coatings: An approach toward process maps. *J. Therm. Spray Technol.* **2014**, *23*, 1009–1018. [[CrossRef](#)]
16. ASTM G32-16 Standard Test Method for Cavitation Erosion Using Vibratory Apparatus; ASTM International: West Conshohocken, PA, USA, 2016.
17. Reza, S.R. Laser surface treatment of Stellite 6 coating deposited by HVOF on 316L alloy. *J. Mater. Eng. Perform.* **2016**, *25*, 2583–2595.
18. Ding, X.; Cheng, X.D.; Yu, X.; Li, C.; Yuan, C.Q.; Ding, Z.X. Structure and cavitation erosion behavior of HVOF sprayed multi-dimensional WC-10Co4Cr coating. *Trans. Nonferrous Met. Soc. China* **2018**, *28*, 487–494. [[CrossRef](#)]
19. Houdková, Š.; Smazalová, E.; Pala, Z. Effect of heat treatment on the microstructure and properties of HVOF-sprayed Co-Cr-W coating. *J. Therm. Spray Technol.* **2016**, *25*, 546–557. [[CrossRef](#)]
20. Sassatelli, P.; Bolelli, G.; Gualtieri, M.L.; Heinonen, E.; Honkanen, M.; Lusvarghi, L.; Manfredini, T.; Rigon, R.; Vippola, M. Properties of HVOF-sprayed Stellite-6 coatings. *Surf. Coat. Technol.* **2018**, *338*, 45–62. [[CrossRef](#)]
21. Ramesh, M.; Prakash, S.; Nath, S.; Sapra, P.K.; Venkataraman, B. Solid particle erosion of HVOF sprayed WC-Co/NiCrFeSiB coatings. *Wear* **2010**, *269*, 197–205. [[CrossRef](#)]
22. Lima, M.; Godoy, C.; Modenesi, P.; Avelar-Batista, J.; Davison, A.; Matthews, A. Coating fracture toughness determined by vickers indentation: An important parameter in cavitation erosion resistance of WC-Co thermally sprayed coatings. *Surf. Coat. Technol.* **2004**, *177*, 489–496. [[CrossRef](#)]
23. Karaoglanli, A.C.; Oge, M.; Doleker, K.M.; Hotamis, M. Comparison of tribological properties of HVOF sprayed coatings with different composition. *Surf. Coat. Technol.* **2017**, *318*, 299–308. [[CrossRef](#)]
24. Lu, J.; Cao, J.; Lu, H.; Zhang, L.; Luo, K. Wear Properties and Microstructural Analyses of Fe-based coatings with various WC contents on H13 die steel by laser cladding. *Surf. Coat. Technol.* **2019**, *369*, 228–237. [[CrossRef](#)]
25. He, M.; Wang, J.; He, R.; Yang, H.; Ruan, J. Effect of cobalt content on the microstructure and mechanical properties of coarse grained WC-Co cemented carbides fabricated from chemically coated composite powder. *J. Alloys Compd.* **2018**, *766*, 556–563. [[CrossRef](#)]
26. Vashishtha, N.; Khatirkar, R.; Sapate, S. Tribological behaviour of HVOF sprayed WC-12Co, WC-10Co-4Cr and Cr₃C₂-25NiCr coatings. *Tribol. Int.* **2017**, *105*, 55–68. [[CrossRef](#)]
27. Hou, G.; Zhao, X.; Zhou, H.; Lu, J.; An, Y.; Chen, J.; Yang, J. Cavitation erosion of several oxy-fuel sprayed coatings tested in deionized water and artificial seawater. *Wear* **2014**, *311*, 81–92. [[CrossRef](#)]

